HHS Public Access

Author manuscript

Mol Cancer Res. Author manuscript; available in PMC 2020 March 01.

Published in final edited form as:

Mol Cancer Res. 2019 March ; 17(3): 751–760. doi:10.1158/1541-7786.MCR-18-0354.

Combinations of Tyrosine Kinase Inhibitor and ERAD Inhibitor Promote Oxidative Stress-Induced Apoptosis through ATF4 and KLF9 in Medullary Thyroid Cancer

Rozita Bagheri-Yarmand[1], **Krishna M. Sinha**[3], **Ling Li**[1], **Yue Lu**[2], **Gilbert J Cote**[1], **Steven I Sherman**[1], **Robert F. Gagel**[1]

[1]Department of Endocrine Neoplasia and Hormonal Disorders, unit 1461

[2]Department of Epigenetics and Molecular Carcinogenesis, unit 0116, The University of Texas MD Anderson Cancer Center, Houston, TX 77030, USA

[3]Department of Orthopaedic Surgery, McGovern Medical School, The University of Texas Health Science Center at Houston, Houston, TX

Abstract

Medullary thyroid carcinoma (MTC) originates from the C cells of the thyroid gland, which secrete calcitonin. Lymph node and distant metastases are frequently present at diagnosis. Activating mutations of *RET*, a driver oncogene in MTC that encodes a tyrosine kinase receptor, prevents apoptosis through inhibition of ATF4, a key transcriptional regulator of endoplasmic reticulum (ER) stress. We hypothesized that the combination of a tyrosine kinase inhibitor (TKI) and an ATF4 inducer promotes cell death by triggering catastrophic oxidative stress and apoptotic cell death. Here, we report that the ER-associated protein degradation (ERAD) inhibitor eeyarestatin sensitized MTC cells to the TKIs, sunitinib and vandetanib, thereby leading to synergistic upregulation of ATF4 expression, accumulation of reactive oxygen species, and subsequent cell death. Genome-wide analysis of ATF4 interaction sites by chromatin immunoprecipitation (ChIP) sequencing revealed that among ATF4 target genes was *KLF9* (Kruppel like factor 9), which induces MTC apoptosis. ChIP assays revealed that ATF4 occupancy at the *KLF9* promoter was increased in MTC cells treated with eeyarestatin or vandetanib alone and was further enhanced in cells treated with both drugs, leading to increased *KLF9* transcription. Depletion of ATF4 by shRNA led to downregulation of *KLF9* expression and prevented oxidative stress-induced cell death. Furthermore, we identified ATF4 target genes (*LZTFL1*, *MKNK2*, and *SIAH1* with known tumor suppressor function) that were synergistically upregulated with the combination of TKI and ERAD inhibitor.

Corresponding author and person to whom reprint requests should be addressed: Rozita Bagheri-Yarmand, Department of Endocrine Neoplasia and Hormonal Disorders, Unit 1461, The University of Texas MD Anderson Cancer Center, Houston, TX 77030, USA. Phone: 713-563-9267, FAX: 713-794-5252, ryarmand@mdanderson.org.

Conflict of interest statement: The authors have no potential conflicts to disclose.

Introduction

Medullary thyroid cancer (MTC) originates from the neuroendocrine C cells of the thyroid gland, which secrete calcitonin. Activating mutations of the *RET* proto-oncogene are the most common drivers of sporadic MTC, identified in 40% to 50% of cases (1). Oncogenic RET protein activates a complex network of signal transduction pathways, that contribute to cellular transformation including the RAF/MAPK/ERK and phosphatidylinositol 3-kinase/AKT pathways (2, 3). MTC is resistant to chemotherapy-induced cell death. Currently, the tyrosine kinase inhibitors (TKIs) cabozantinib and vandetanib are approved by the US Food and Drug Administration for the treatment of advanced, progressive, or symptomatic MTC (4). However, responses to these agents are incomplete, often unsustainable and resistance develops (5, 6). These TKIs increases mitochondrial membrane potential and causes bioenergetics stress and their combination with mitochondrial-targeted agents suppresses MTC tumor growth in mice (7). In addition, targeting mitochondrial chaperone such as HSPA9 (GRP75/Mortalin) suppress human MTC cells in culture and in mouse xenografts (8).

Cancer cells with high secretory function, such as the parafollicular C cells that secrete calcitonin and other peptides, are more dependent on the quality control provided by the ubiquitin-proteasome system. Proteasome inhibitors that target the ubiquitin-proteasome system have been proven to be effective against hematologic malignancies, also active secretory cells (9). Thus, targeting protein homeostasis pathways could be exploited for the treatment of tumors with high protein synthesis rate. Endoplasmic reticulum (ER)-associated protein degradation (ERAD) controls the quality of glycosylated and nonglycosylated protein in the ER and eliminates misfolded and unassembled proteins (10). Accumulation of unfolded proteins that are not resolved triggers cell death (11). Eeyarestatin I (hereafter, “eeyarestatin”) is an ERAD inhibitor that disturbs ER homeostasis and has anticancer activities resembling that of the proteasome inhibitor, bortezomib (12). Eeyareatatin directly binds the p97 ATPase, a key regulator of ERAD machinery, to inhibit p97 binding to the ER membrane and thereby induce cell death through ATF4, ATF3, and NOXA (13). One mechanism underlying the chemoresistance of MTC is that RET prevents apoptosis through phosphorylation-dependent inhibition of ATF4 transcriptional activity (14). We recently demonstrated that treatment of MTC cells with TKIs enhances ATF4 protein levels and activation of ATF4 target genes (14). ATF4 promotes the induction of apoptosis under persistent stress conditions, although the mechanism is not clearly understood. We hypothesized that the combination of an ATF4 inducer and a TKI causes excessive cellular oxidative stress resulting in the activation of apoptosis.

In the present study, we demonstrated that combinations of TKIs and eeyarestatin synergistically induced apoptosis in MTC cells in vitro through an increase in reactive oxygen species (ROS) and upregulation of ATF4 and ATF4 target genes. These findings provide a preclinical rationale for further evaluation of combinations of TKIs and ERAD inhibitors for MTC in a clinical trial. This combination therapy requires lower doses of TKIs than are required with single-agent TKI therapy and may increase efficacy and reduce side effects while preventing resistance to TKIs and thereby enhancing the survival of patients with MTC.

Materials and Methods

Reagents and antibodies.

Eeyarestatin, sunitinib and vandetanib were purchased from Tocris Bioscience. Antibodies specific to BBC3 (D30C10) and MCL1 (D35A5) were purchased from Cell Signaling Technology. PMAIP1 (114C307) antibody was purchased from Calbiochem. ATF4 (D4B8) antibody was purchased from Abcam. RET (C-20), SIAH1 (N-15), and MNK2 (S-20) antibodies were purchased from Santa Cruz Biotechnology. Anti-active caspase 3 and anti-cleaved PARP (ASP214) were purchased from BD Biosciences.

Cell lines.

Two MTC cell lines, TT and MZCRC1, were used. TT cells were purchased from ATCC. MZCRC1 cells were kindly provided by Dr. Alex Knuth (Switzerland) and were previously described (15-17). RET mutations in MTC cell lines were verified by sequencing; the codon 918 in exon 16 of *RET* gene (methionine is mutated to threonine) RET-M918T in MZCRC1 cells and the codon 634 in exon 11 of *RET* gene (cysteine is mutated to tryptophan) RET-C634W in TT cells. All cell lines were tested negative for mycoplasma using the service provided by the core facility at MDACC. Cells used for the experiments were between 2 to 5 passages from thawing.

Plasmid construction and lentiviral transduction.

Lentiviral vectors (pLKO.1) containing ATF4-specific shRNAs were purchased from Sigma-Aldrich. Lentiviral ATF4-shRNA plasmids were co-transfected into HEK293T cells along with packaging (VPR8.9) and envelope (VSV-G) plasmids using X-tremeGENE (Roche) for 2 days. The virus particles containing ATF4-shRNA or control shRNA were used to infect TT cells. Transfected cells were selected in media containing 2 μg/mL puromycin (Clontech).

Cell viability, and apoptosis analyses.

For cell viability assay, 40,000 cells were plated per well in a 96-well plate and treated as indicated with various drug combinations for different time points. Then, the cells were treated with 200 μl of 0.6 mg/ml MTT (3-(4,5-Dimethylthiazol-2-yl)-2,5-diphenyltetrazolium bromide, a tetrazole) in serum-free medium for 4 h, and then solubilized in dimethyl sulfoxide for 30 min and absorbance was measured with a spectrophotometer (Synergy HT; BioTek) at 595 nm. The percent of apoptotic cells was measured using a BD ApoAlert Annexin V-FITC apoptosis kit (BD Biosciences) according to the manufacturer's instructions, and cells were analyzed on a FACscan system (Becton Dickinson). Additionally, cells were fixed, stained with antibodies against cleaved caspase 3 and cleaved PARP, and analyzed by flow cytometry.

Drug-combination data analysis.

The degree of synergism between the eeyarestatin and TKIs was determined using CompuSyn software, version 1 (ComboSyn, Inc.)(18). The combination index for each combination was calculated at a nonconstant ratio and was used to express synergism (CI<

1), additivity (CI = 1) or antagonism (CI > 1). Normalized isobologram for non-constant combinations ratios is presented.

Measurement of ROS.

Cells were collected after trypsinization, washed with serum-free medium, and resuspended in 500 μl of serum-free medium containing 10 μM of the redox-sensitive fluorescent dye 5-(and 6)-carboxy-2', 7'-dichlorodihydrofluorescein diacetate (carboxy-H2DCFDA) (Sigma). Cells were incubated at 37°C for 30 min, pelleted at 1200 rpm for 5 min, and resuspended in 500 μl of serum-free medium. Samples were analyzed on a Beckman Coulter Gallios flow cytometer. Data were analyzed with FlowJo software version 10.3), and mean fluorescence intensity was obtained.

Real-time PCR.

RNA and cDNA were prepared using a Cells-to-CT kit (Invitrogen). Quantitative PCR was performed with a polymerase-activating/DNA-denaturing step of 95°C for 15 s and 60°C annealing/elongation step for 1 min on a StepOne real-time PCR system (Applied Biosystems). TaqMan primer-probes were purchased from Applied Biosystems. Gene expression values were normalized to HPRT mRNA.

Chromatin immunoprecipitation (ChIP) and ChIP sequencing (ChIP-seq) assay.

MZCRC1 cells were treated with eeyarestatin (5 μM) for 16 h, and ChIP assay was performed as described previously (14). For ChIP-seq, sequencing libraries are made up of random fragments that represent the entire sample. Libraries are created by shearing DNA (Covaris S220) into 150-bp to 400-bp fragments. These fragments are ligated to specific adapters. Library fragments of the appropriate size are then selected and isolated. Following a sample clean-up step, the resulting library is quantified by qPCR and checked for quality using the Agilent Bioanalyzer.

The libraries were pooled and sequenced on the Illumina Hiseq-2000 platform at the sequencing and microarray facility of The University of Texas MD Anderson Cancer Center. ChIP-seq reads were aligned to the human genome assembly, and the ChIP-seq peaks were called using MACS 2.0. Regions of enrichment comparing ChIP and input control signal exceeding $q<0.01$ were called as peaks. The primers used to amplify the indicated genes are shown in Table S1 in Supplementary Materials and Methods.

Biochemical assays.

Western blot analysis and immunoprecipitation were performed as described previously (19).

Statistical analysis.

All data were expressed as mean ± standard deviation. Data were analyzed with GraphPad Prism7 software using the indicated tests. Statistical significance was indicated as follows: *, $P<0.05$; **, $P<0.01$; ***, $P<0.001$; and ****, $P<0.0001$.

Results

ERAD inhibitor eeyarestatin induces apoptosis of MTC cells.

ERAD eliminates misfolded or unassembled proteins from the ER. ERAD targets are exported from the ER to the cytoplasm and degraded by the ubiquitin-proteasome system (20). Eeyarestatins are ERAD-specific inhibitors that elicit an integrated stress response program at the ER resulting in activation of ATF4 which subsequently stimulates expression of the apoptotic gene *PMAIP1* (*NOXA*), which results in cell death (12, 13). Because of the secretory nature of MTC cells, we hypothesized that a compound that induces ER stress and overwhelms the hyperactive secretory pathway in MTC cells will induce apoptotic cell death. Eeyarestatin (EE) has previously been reported to induce cell death in various other cancers (12). We first tested whether EE could induce cell death in the MTC cell lines TT and MZCRC1. The viability of MTC cells treated with EE at increasing concentration for 48 h was measured by a colorometric assay using MTT and annexin V/FITC staining. Eeyarestatin induced cell death in these cells but MZCRC1 cells were less sensitive than TT cells (Fig. 1A, B). Furthermore, in both MTC cell lines, treatment with eeyarestatin increased mRNA levels of genes involved in the UPR and apoptotic pathways, including *ATF4*, *DDIT3* (*CHOP*), *TRIB3*, *SESN2*, *BBC3* (*PUMA*), and *PMAIP1* (*NOXA*) with greater induction in TT cells compared to MZCRC1 cells (Fig. 1C). The mRNA level of *RET* proto-oncogene was not affected (Fig. 1C). We previously reported that ATF4 overexpression promotes RET degradation (21). Thus, we reasoned that eeyarestatin might promote RET degradation through ATF4 activation. As expected, in eeyrarestatin-treated TT cells, the level of ATF4 protein increased while the level of RET protein completely abrogated (Fig. 1D). We observed similar results in EE-treated MZCRC1 cells but the effect of EE on the levels of ATF4 and RET was moderate compared to TT cells (Fig. 1E).

Combinations of ERAD inhibitor eeyarestatin and a TKI synergistically induce apoptosis of MTC cells through ROS accumulation.

Although the TKIs sunitinib and vandetanib are effective for the treatment of MTC, patients often develop resistance to these drugs (5, 6, 22). We previously reported that vandetanib increases ATF4 transcriptional activity (14). Transcriptional induction of ATF4 and CHOP increases protein synthesis, leading to oxidative stress and cell death (23). ROS accumulation has been reported to trigger ER stress and the UPR, which in turn induce apoptosis through activation of ER stress-mediated apoptotic pathways (24, 25). We hypothesized that eeyarestatin inhibits the degradation of misfolded proteins, leading to severe UPR and that the combination of eeyarestatin with a TKI synergistically enhances ER stress and ROS accumulation, leading to apoptosis. Using MTT assay, we observed decreased viability of MTC cells (TT and MZCRC1) treated with various doses of eeyarestatin alone (0.1–6 μM) or sunitinib or vandetanib alone (0.1–1 μM) and increased cytotoxicity when cells were treated with combinations of eeyarestatin and either sunitinib or vandetanib (Fig. 1F, G). Calculation of the drug combination index showed that the combinations of eeyarestatin with sunitinib or vandetanib had synergistic cytotoxic effects (Table S1). Normalized isobologram with non-constant combinations ratios are shown for the combination of eeyarestatin and vandetanib in TT (Fig. 1H and1I).

To investigate whether the combination of eeyarestatin and a TKI causes apoptosis, we quantified the fraction of apoptotic cells by counting cleaved caspase 3–positive and cleaved PARP–positive cells by flow cytometry. Co-treatment of TT cells with eeyarestatin and sunitinib or vandetanib triggered substantial apoptosis in a manner that was not observed after treatment with eeyarestatin, sunitinib or vandetanib alone (Fig. 2A, B). For example, cells treated with 4μM eeyarestatin, vandetanib or sunitinib alone induced 11.4 % ± 1.98 (n=3); 7.24% ± 3.37 (n=3); 16.45% ± 5 (n=3) cell death respectively (Fig. 2B). Combination treatment with 4μM of eeyarestatin and 4μM vandetanib or sunitinib for 24 hours yielded 52% ± 9.2: 48% ± 0.4 cells death, respectively (Fig. 2B). The MZCRC1 cells showed less sensitivity to the combination of vandetanib with eeyarestatin compared to TT cells (Fig. S1). MTC cell lines contain a self-renewing CD133 population that is dependent on RET protooncogene. MZCRC1 cells, which harbors an M918*RET* mutation, has a greater CD133 cell number and sphere-forming ability than the TT cell line, which harbors C634W mutation (15). We sought to test the combination therapy in MZCRC1 spheres. We found that the combination of eeyaresatin and sunitinib caused asynergistic cell death on MZCRC1 spheres more efficiently than monolayer cells (Fig. S2).

We have previously reported that vandetanib treatment to MTC cells led to increased expression of ATF4 (14). We next examined whether ATF4 knockdown in TT cells decreased drug-induced apoptosis. TT-shRNA-ATF4 stable cell lines were previously described (21). We showed that in ATF4-depleted TT cells (shRNA-ATF4 #74 and #76), apoptotic response to either eeyarestatin or the combination of eeyarestatin and sunitinib or vandetanib was significantly decreased compared to the response in parental cells without ATF4 depletion (Fig. 2A, B). Western blot analysis confirmed an increased expression of ATF4 and its proapoptotic targets BBC3 (PUMA) and PMAIP1 (NOXA) in TT cells treated with sunitinib and eeyarestatin than in TT cells treated with a single drug (Fig. 2C). In contrast, expression levels of survival factor MCL1 decreased significantly more in cells treated with the combination than in cells with single drug treatment (Fig. 2C). These results suggested that the combination of ATF4 inducer and a TKI causes synergistic activation of apoptosis.

We next determined whether eeyarestatin and TKIs cooperatively induced oxidative stress in MTC cells. We detected significantly increased carboxy-H2DFDA fluorescence in sunitinib-treated or eeyarestatin-treated cells compared to control cells (Fig. 3A). The combination of sunitinib and eeyarestatin triggered a greater increase in fluorescence (Fig. 3A, B). We reasoned that ATF4 induction contributes to the effects of this drug combination. Indeed, ATF4 knockdown abolished ROS accumulation which was induced by sunitinib, eeyarestatin and their combination (Fig. 3A, B). Enhanced ROS accumulation was also observed in MZCRC1 cells treated with eeyarestatin, sunitinib or vandetanib and their combination (Fig. 3C). Furthermore, ROS scavenger (n-acetyl cysteine (NAC) decreased ROS accumulation and cell death in MTC cells treated with eeyarestatin or vandetanib (Fig. 3C). Together these results suggest that excessive oxidative stress, a physiological response triggered by these drugs, is required for the observed cytotoxicity (Fig. 3C).

ATF4 induces target genes involved in the UPR, apoptosis, transcription, and oxidative stress.

To identify the ATF4 transcriptional targets involved in oxidative stress, we performed ChIP-seq assay in MZCRC1 cells treated with eeyarestatin. Chromatins were prepared from treated cells and immunoprecipitated with antibodies specific for ATF4 or H3K9AC, an active histone marker that correlates with gene activation. Precipitated DNA was purified and then used for sequencing with the Illumina Hiseq-2000 platform; the resulting sequences were aligned to the human genome. Peaks containing ATF4 and H3K9AC binding regions were viewed with Integrative Genomics Viewer version 2.3. Relative enrichment and density mapping plots indicated that ATF4 and H3K9AC binding sites were enriched around the promoter regions (Fig. 4A). A total of 512 unique peaks were found after removal of nonspecific genes (26 peaks) (p-value 1.00E-07 and false discovery rate 0.5). Analysis of distribution of these 512 unique peaks in the genome showed that 18.4% of the peaks were upstream of the transcription start site, 22.1% were at the promoter, 2.9% were in the exon region, 29.1% were in the intronic region, 2.1% were in the transcription end site, 8.6% were downstream of the transcription start site, and 16.8% were in distant regions (Fig. 4B). Moreover, 52% of the ATF4 peaks overlapped with H3K9AC peaks, mostly in the promoter regions, and 55.3% of H3K9AC peaks (a total of 22,339 peaks) lay at the promoter region. Next, we performed motif analyses of the ATF4 binding sites using the MEME-ChIP program. The ATGC frequency in the canonical motifs is shown for ATF4 binding sites to demonstrate motif conservation (Fig. 4C). Taken together, these ChIP-seq findings provided a precise genomewide view of ATF4 binding upon ER stress induced by eeyarestatin. Ingenuity Pathway Analysis of the ATF4 target genes revealed enrichment of genes involved in the UPR, ER stress pathway, EIF2 signaling, cell death pathway, ERK/MAPK signaling, p38 MAPK signaling, PI3kinase mTOR pathways, TR/RXR activation, and NRF2-mediated oxidative stress response (Supplementary Fig. S3, Table S3).

The occupancy of ATF4 at the promoter of several known (*DDIT3*, *BBC3*) and previously unknown target genes (*SIAH1*, *MKNK2, LZTFL1*) was further validated by manual ChIP in MZCRC1 cells treated with eeyarestatin, vandetanib or their combination (Fig. 4D, Table S3, Figure S4). Leucine zipper transcription factor-like 1 (*LZTFL1*) has been shown to inhibit TGFβ-activated MAPK, hedgehog signaling, and β−catenin–Wnt signaling pathway, acting as a tumor suppressor gene in lung and gastric cancer (26). *MKNK2* is downregulated in human cancers and is a tumor suppressor that activates p38-MAPK, leading to p38-mediated cell death (27). *SIAH1* is a p53-inducible mediator of cell cycle arrest, tumor suppression, and apoptosis (28). We found that the combination of eeyarestatin and vandetanib increased the occupancy of ATF4 at the promoter of *DDIT3*, *BBC3*, *SIAH1*, *MKNK2*, and *LZTFL1* genes more than either single treatment did (Fig. 4D). Gene expression analyses showed that in TT or MZCRC1 cells treated with eeyarestatin, sunitinib or vandetanib, as well as their combination, the mRNA levels of *ATF4* and ATF4 target genes were more induced with the combination of these drugs than sunitinib, vandetanib and eeyarestatin alone (Fig. 5A-C)). Western blot analysis further confirmed increased protein levels of LZTFL1, SIAH1, and MKNK2 in MZCRC1 cells treated with eeyarestatin, sunitinib, and the two drugs in combination (Fig. 5D).

KLF9 is a downstream target of ATF4.

ChIP-seq analysis revealed that ATF4 binds to the promoter and enhancer region of *KLF9* (Fig. 6A-C). KLF9 is a member of the SP1 C2H2-type zinc finger family of transcription factors and is ubiquitously expressed in various tissues (29). KLF9 is upregulated by oxidative stress, which causes accumulation of ROS and promotes oxidative stress-induced cell death (30). Using ChIP assay, we confirmed the ATF4 binding to the promoter of *KLF9* using the specific primers flanking the ATF4 peaks within the promoter and enhancer regions. We found that ATF4 occupancy at the *KLF9* promoter or enhancer regions was significantly increased in MZCRC1 cells treated with eeyarestatin alone or vandetanib alone compared to untreated cells (Fig. 6B, C). The combination increased the ATF4 occupancy compared to single drug treatment (Fig. 6B, C). Expression analysis by quantitative RT-PCR revealed that the combination treatment had enhanced expression levels of the *KLF9* gene compared to single drug treatment in MZCRC1 cells (Fig. 6D). To determine whether upregulation of ATF4 plays a functional role in the induction of *KLF9* upon treatment, ATF4 was stably downregulated in TT and MZCRC1 cells by shRNA, and then cells were treated with eeyarestatin (Fig. 6E-G). ATF4 knockdown prevented EE-induced upregulation of *KLF9* gene (Fig. 6F-G) and oxidative stress-induced cell death (Fig. 3B). Western blot analysis confirmed that KLF9 expression was upregulated by eeyarestatin and sunitinib alone and further upregulated by the combination (Fig. 6H). Altogether our results indicate that ATF4 induction activates the transcription of *KLF9* gene and induces oxidative stress mediated cell death.

Discussion

In the work reported herein, we identified a promising drug combination that functions by triggering irresolvable oxidative stress and apoptosis in response to ER stress. Our data demonstrate that in MTC cells, combinations of the ERAD inhibitor eeyarestatin and a TKI, either sunitinib or vandetanib, synergistically induced a high level of ATF4 expression. Among the ATF4 target genes activated by this drug combination, we identified *KLF9*, which has been reported to regulate intracellular ROS (32), as a novel ATF4 target gene.

ROS production in cancer cells is one of the mechanisms underlying synergistic cytotoxicity of combination therapies (33, 34). Cancer cells exhibit higher levels of ROS than normal cells, and these higher levels of ROS increase the sensitivity of cancer cells to drugs that further increase ROS levels and oxidative stress (35). In response to oxidative stress, accumulation of unfolded or misfolded protein triggers ER stress, thereby enabling amplification loops that may contribute to the switch from adaptive to fatal UPR (36). Our findings showed that both vandetanib and eeyarestatin increased ATF4 recruitment to the *KLF9* promoter and that recruitment was even greater when the two drugs were combined, which consequently results in induction of *KLF9* at both mRNA and proteins levels and ROS production, leading to increased apoptosis. It has been reported that KLF9 causes intracellular ROS accumulation partly by suppressing the transcription of the thioredoxin reductase 2 gene (*TXNRD2*), which plays a critical role in defense against oxidative damage (30). It is shown that cytotoxicity mediated by the stress-inducing agents, the histone deacetylase inhibitor panobinostat and the proteasome inhibitor bortezomib is through

increased expression of KLF9 (31). Our data suggest a model of ATF4-dependent regulation of ROS through upregulation of KLF9 that is sufficient to cause cell death. The similar feed-forward regulatory loop is previously reported in response to DNA damage or oxidative stress (37, 38).

It has been shown that ATF4 mediates ER stress-induced apoptosis in response to compounds triggering ER stress, such as an inhibitor of ATPase p97 (39); HA15 (a thiazole benzenesulfonamide), which targets GRP78/Bip (40); fenretinide; and the proteasome inhibitor bortezomib (41). Furthermore, ATF4 knockdown reduced vemurafenib-induced apoptosis (42).

ERAD inhibitor eeyarestatin directly binds to the p97 ATPase complex, a key regulator of protein homeostasis, and inhibits deubiquitination of substrates, leading to accumulation of polyubiquitinated proteins in cells, which induces ER stress and subsequent cell death (39). P97 inhibitor exerts strong antitumor activity in several solid tumors by inducing UPR and irresolvable proteotoxic stress leading to cancer cell death (39). Interestingly, eeyarestatin seems to induce moderate ER stress in normal cells without inducing cell death, supporting the idea that cancer cells are more sensitive than normal cells to perturbations of ER homeostasis(43). Because MTC originates from the C cells of the thyroid gland, which secrete calcitonin, MTC cells are highly reliant on their UPR and ERAD pathways as a result of their high protein synthesis burden; this may explain why MTC cells are more sensitive to ER stress inducers than are cancer cells with no secretory function. Thus, increasing ATF4 expression in MTC tumors may constitute a therapeutic strategy for inhibiting tumor growth through increasing the expression of tumor suppressor genes.

In summary, as increased ER stress is common in most types of human tumors, inducing ER stress and oxidative stress sufficiently to induce death of cancer cells but not normal cells could be a useful new approach to cancer treatment.

Supplementary Material

Refer to Web version on PubMed Central for supplementary material.

Acknowledgments

This work was supported by the National Institutes of Health through grants P50CA168505/DRP (to R. B.Y), Cancer Center Support Grant (CA016672), Kosberg Foundation (to R. F. G). We thank the department of Scientific Publication at MD Anderson for editing the manuscript.

References

1. Romei C, Ciampi R, Elisei R A comprehensive overview of the role of the RET proto-oncogene in thyroid carcinoma. Nature reviews Endocrinology. 2016;12(4):192–202.
2. Takahashi M The GDNF/RET signaling pathway and human diseases. Cytokine Growth Factor Rev. 2001;12(4):361–73. [PubMed: 11544105]
3. van Weering DH, Bos JL. Signal transduction by the receptor tyrosine kinase Ret. Recent Results Cancer Res. 1998;154:271–81. [PubMed: 10027007]

4. Phay JE, Shah MH. Targeting RET receptor tyrosine kinase activation in cancer. Clinical cancer research : an official journal of the American Association for Cancer Research. 2010;16(24):5936–41. [PubMed: 20930041]
5. Wells SA Jr., Robinson BG, Gagel RF, Dralle H, Fagin JA, Santoro M, et al. Vandetanib in patients with locally advanced or metastatic medullary thyroid cancer: a randomized, double-blind phase III trial. Journal of clinical oncology : official journal of the American Society of Clinical Oncology. 2012;30(2):134–41. [PubMed: 22025146]
6. Elisei R, Schlumberger MJ, Muller SP, Schoffski P, Brose MS, Shah MH, et al. Cabozantinib in progressive medullary thyroid cancer. Journal of clinical oncology : official journal of the American Society of Clinical Oncology. 2013;31(29):3639–46. [PubMed: 24002501]
7. Starenki D, Hong SK, Wu PK, Park JI. Vandetanib and cabozantinib potentiate mitochondria-targeted agents to suppress medullary thyroid carcinoma cells. Cancer biology & therapy. 2017;18(7):473–83. [PubMed: 28475408]
8. Starenki D, Hong SK, Lloyd RV, Park JI. Mortalin (GRP75/HSPA9) upregulation promotes survival and proliferation of medullary thyroid carcinoma cells. Oncogene. 2015;34(35):4624–34. [PubMed: 25435367]
9. Miller Z, Ao L, Kim KB, Lee W. Inhibitors of the immunoproteasome: current status and future directions. Current pharmaceutical design. 2013;19(22):4140–51. [PubMed: 23181576]
10. Araki K, Nagata K. Protein folding and quality control in the ER. Cold Spring Harbor perspectives in biology. 2011;3(11):a007526. [PubMed: 21875985]
11. Pakos-Zebrucka K, Koryga I, Mnich K, Ljujic M, Samali A, Gorman AM. The integrated stress response. EMBO reports. 2016;17(10):1374–95. [PubMed: 27629041]
12. Wang Q, Mora-Jensen H, Weniger MA, Perez-Galan P, Wolford C, Hai T, et al. ERAD inhibitors integrate ER stress with an epigenetic mechanism to activate BH3-only protein NOXA in cancer cells. Proceedings of the National Academy of Sciences of the United States of America. 2009;106(7):2200–5. [PubMed: 19164757]
13. Wang Q, Shinkre BA, Lee JG, Weniger MA, Liu Y, Chen W, et al. The ERAD inhibitor Eeyarestatin I is a bifunctional compound with a membrane-binding domain and a p97/VCP inhibitory group. PloS one. 2010;5(11):e15479. [PubMed: 21124757]
14. Bagheri-Yarmand R, Sinha KM, Gururaj AE, Ahmed Z, Rizvi YQ, Huang SC, et al. A novel dual kinase function of the RET proto-oncogene negatively regulates activating transcription factor 4-mediated apoptosis. The Journal of biological chemistry. 2015;290(18):11749–61. [PubMed: 25795775]
15. Zhu W, Hai T, Ye L, Cote GJ. Medullary thyroid carcinoma cell lines contain a self-renewing CD133+ population that is dependent on ret proto-oncogene activity. The Journal of clinical endocrinology and metabolism. 2010;95(1):439–44. [PubMed: 19897677]
16. Vitagliano D, De Falco V, Tamburrino A, Coluzzi S, Troncone G, Chiappetta G, et al. The tyrosine kinase inhibitor ZD6474 blocks proliferation of RET mutant medullary thyroid carcinoma cells. Endocr Relat Cancer. 2011;18(1):1–11. [PubMed: 20943719]
17. Cooley LD, Elder FF, Knuth A, Gagel RF. Cytogenetic characterization of three human and three rat medullary thyroid carcinoma cell lines. Cancer Genet Cytogenet. 1995;80(2):138–49. [PubMed: 7736432]
18. Chou TC. Drug combination studies and their synergy quantification using the Chou-Talalay method. Cancer research. 2010;70(2):440–6. [PubMed: 20068163]
19. Hsu SC, Hung MC. Characterization of a novel tripartite nuclear localization sequence in the EGFR family. The Journal of biological chemistry. 2007;282(14):10432–40. [PubMed: 17283074]
20. Meusser B, Hirsch C, Jarosch E, Sommer T. ERAD: the long road to destruction. Nature cell biology. 2005;7(8):766–72. [PubMed: 16056268]
21. Bagheri-Yarmand R, Williams MD, Grubbs EG, Gagel RF. ATF4 Targets RET for Degradation and Is a Candidate Tumor Suppressor Gene in Medullary Thyroid Cancer. The Journal of clinical endocrinology and metabolism. 2017;102(3):933–41. [PubMed: 27935748]
22. Dadu R, Hu MN, Grubbs EG, Gagel RF. Use of Tyrosine Kinase Inhibitors for Treatment of Medullary Thyroid Carcinoma. Recent results in cancer research. 2015;204:227–49. [PubMed: 26494392]

23. Han J, Back SH, Hur J, Lin YH, Gildersleeve R, Shan J, et al. ER-stress-induced transcriptional regulation increases protein synthesis leading to cell death. Nature cell biology. 2013;15(5):481–90. [PubMed: 23624402]
24. Kuznetsov JN, Leclerc GJ, Leclerc GM, Barredo JC. AMPK and Akt determine apoptotic cell death following perturbations of one-carbon metabolism by regulating ER stress in acute lymphoblastic leukemia. Molecular cancer therapeutics. 2011;10(3):437–47. [PubMed: 21262957]
25. Quan Z, Gu J, Dong P, Lu J, Wu X, Wu W, et al. Reactive oxygen species-mediated endoplasmic reticulum stress and mitochondrial dysfunction contribute to cirsimaritin-induced apoptosis in human gallbladder carcinoma GBC-SD cells. Cancer letters. 2010;295(2):252–9. [PubMed: 20359814]
26. Wei Q, Chen ZH, Wang L, Zhang T, Duan L, Behrens C, et al. LZTFL1 suppresses lung tumorigenesis by maintaining differentiation of lung epithelial cells. Oncogene. 2016;35(20): 2655–63. [PubMed: 26364604]
27. Maimon A, Mogilevsky M, Shilo A, Golan-Gerstl R, Obiedat A, Ben-Hur V, et al. Mnk2 alternative splicing modulates the p38-MAPK pathway and impacts Ras-induced transformation. Cell reports. 2014;7(2):501–13. [PubMed: 24726367]
28. Liu J, Stevens J, Rote CA, Yost HJ, Hu Y, Neufeld KL, et al. Siah-1 mediates a novel beta-catenin degradation pathway linking p53 to the adenomatous polyposis coli protein. Molecular cell. 2001;7(5):927–36. [PubMed: 11389840]
29. Kikuchi Y, Sogawa K, Watanabe N, Kobayashi A, Fujii-Kuriyama Y. Purification and characterization of the DNA-binding domain of BTEB, a GC box-binding transcription factor, expressed in Escherichia coli. Journal of biochemistry. 1996;119(2):309–13. [PubMed: 8882723]
30. Zucker SN, Fink EE, Bagati A, Mannava S, Bianchi-Smiraglia A, Bogner PN, et al. Nrf2 amplifies oxidative stress via induction of Klf9. Molecular cell. 2014;53(6):916–28. [PubMed: 24613345]
31. Mannava S, Zhuang D, Nair JR, Bansal R, Wawrzyniak JA, Zucker SN, et al. KLF9 is a novel transcriptional regulator of bortezomib- and LBH589-induced apoptosis in multiple myeloma cells. Blood. 2012;119(6):1450–8. [PubMed: 22144178]
32. Tetreault MP, Yang Y, Katz JP. Kruppel-like factors in cancer. Nature reviews Cancer. 2013;13(10): 701–13. [PubMed: 24060862]
33. Zou P, Chen M, Ji J, Chen W, Chen X, Ying S, et al. Auranofin induces apoptosis by ROS-mediated ER stress and mitochondrial dysfunction and displayed synergistic lethality with piperlongumine in gastric cancer. Oncotarget. 2015;6(34):36505–21. [PubMed: 26431378]
34. Zou P, Xia Y, Chen W, Chen X, Ying S, Feng Z, et al. EF24 induces ROS-mediated apoptosis via targeting thioredoxin reductase 1 in gastric cancer cells. Oncotarget. 2016;7(14):18050–64. [PubMed: 26919110]
35. Trachootham D, Alexandre J, Huang P. Targeting cancer cells by ROS-mediated mechanisms: a radical therapeutic approach? Nature reviews Drug discovery. 2009;8(7):579–91. [PubMed: 19478820]
36. Tabas I, Ron D. Integrating the mechanisms of apoptosis induced by endoplasmic reticulum stress. Nature cell biology. 2011;13(3):184–90. [PubMed: 21364565]
37. Biton S, Ashkenazi A. NEMO and RIP1 control cell fate in response to extensive DNA damage via TNF-alpha feedforward signaling. Cell. 2011;145(1):92–103. [PubMed: 21458669]
38. Rocourt CR, Wu M, Chen BP, Cheng WH. The catalytic subunit of DNA-dependent protein kinase is downstream of ATM and feeds forward oxidative stress in the selenium-induced senescence response. The Journal of nutritional biochemistry. 2013;24(5):781–7. [PubMed: 22841545]
39. Anderson DJ, Le Moigne R, Djakovic S, Kumar B, Rice J, Wong S, et al. Targeting the AAA ATPase p97 as an Approach to Treat Cancer through Disruption of Protein Homeostasis. Cancer cell. 2015;28(5):653–65. [PubMed: 26555175]
40. Cerezo M, Lehraiki A, Millet A, Rouaud F, Plaisant M, Jaune E, et al. Compounds Triggering ER Stress Exert Anti-Melanoma Effects and Overcome BRAF Inhibitor Resistance. Cancer cell. 2016;30(1):183.
41. Armstrong JL, Flockhart R, Veal GJ, Lovat PE, Redfern CP. Regulation of endoplasmic reticulum stress-induced cell death by ATF4 in neuroectodermal tumor cells. The Journal of biological chemistry. 2010;285(9):6091–100. [PubMed: 20022965]

42. Beck D, Niessner H, Smalley KS, Flaherty K, Paraiso KH, Busch C, et al. Vemurafenib potently induces endoplasmic reticulum stress-mediated apoptosis in BRAFV600E melanoma cells. Science signaling. 2013;6(260):ra7. [PubMed: 23362240]

43. Yadav RK, Chae SW, Kim HR, Chae HJ. Endoplasmic reticulum stress and cancer. Journal of cancer prevention. 2014;19(2):75–88. [PubMed: 25337575]

Implication:

These findings reveal a combination therapy that induces reactive oxygen species-dependent catastrophic cell death through induction of ATF4 and KLF9 transcriptional activity.

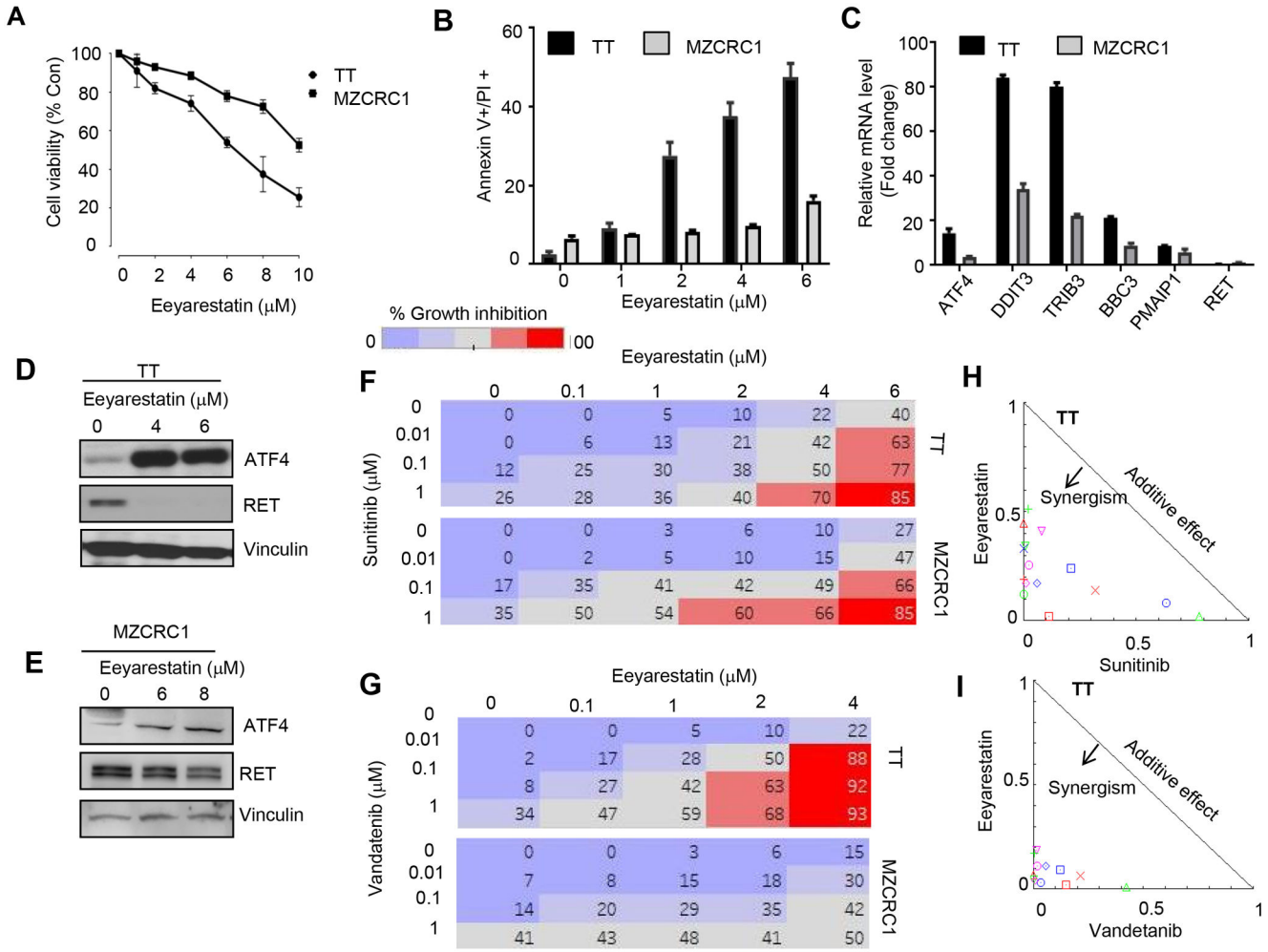

Figure 1.

Synergistic cytotoxic effects of combinations of eeyarestatin with sunitinib or vandetanib in MTC cells. **A,** Cytotoxic activity of eeyarestatin in TT and MZCRC1 cells. Cells were treated as indicated for 48 h, and cell viability was measured by an MTT assay. Data presented as the mean of three independent experiments. Error bars, ±SD (n=3). **B,** Eeyarestatin induces cell death. TT or MZCRC1 cells were treated as indicated for 48 h, dead cells were quantified using an annexin V/propidium iodide (PI) assay by flow cytometry. Data presented as the mean of three independent experiments. Error bars, ±SD (n=3). *p<0.05, **p<0.01 (unpaired two-tailed t-test). **C,** Eeyarestatin activates *ATF4* and its target genes in TT and MZCRC1 cells. Quantitative real-time PCR showing mRNA levels of indicated genes using HPRT mRNA as an internal control. Error bars, ±SD (n=3). **D**, **E,** TT or MZCRC1 cells were treated with eeyarestatin for 48 h at indicated doses; immunoblot depicts ATF4 and RET expression. Vinculin served as a loading control. **F, G.** MTT assay of TT and MZCRC1 cells treated with eeyarestatin, sunitinib, vandetanib or their combination as indicated for 48 h. Percentage inhibition at each concentration of the drugs in TT and MZCRC1 cells is shown. Data presented as the mean of three independent experiments. Error bars, ±SD (n=3). **H, I,** normalized Isobologram for non-constant ratios for eeyarestatin

combination with sunitinib or vandetanib in TT cells were obtained using CompuSyn software, which performs drug dose-effect calculation using the median effect method.

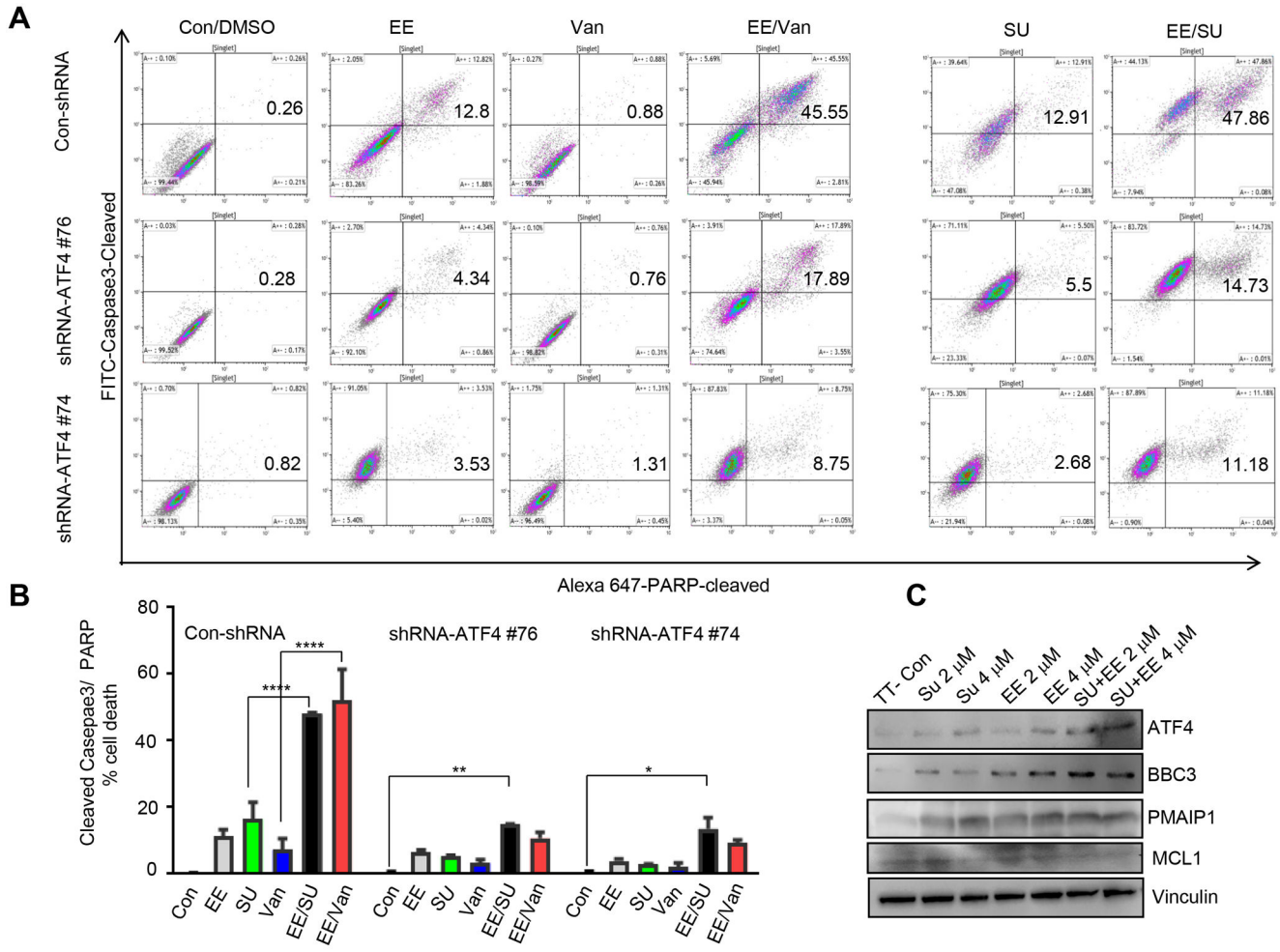

Figure 2.

Eeyarestatin in combination with either sunitinib or vandetanib synergistically induce cell death. **A,** Cleaved caspase 3–positive and cleaved PARP–positive cells were quantified using flow cytometry after treatment of TT cells or TT-shRNA-ATF4 clone #74, #76 with eeyarestatin alone(4µM), vandetanib alone(4µM), sunitinib (4µM) alone, or their combinations for 24 h. **B,** Cumulative analysis of cell death as described in A from three independent experiments. The data presented as mean± SD. The statistical analysis used was a two-way analysis of variance (Tukey's multiple comparisons test). $*P < 0.05$, $**P < 0.01$, $****P < 0.0001$. **C**, Western blot showing levels of apoptotic and survival proteins in control cells and cells treated for 48 h as indicated. Vinculin served as a loading control. Con, control non treated cells; EE, eeyarestatin; SU, sunitinib, Van, vandetanib

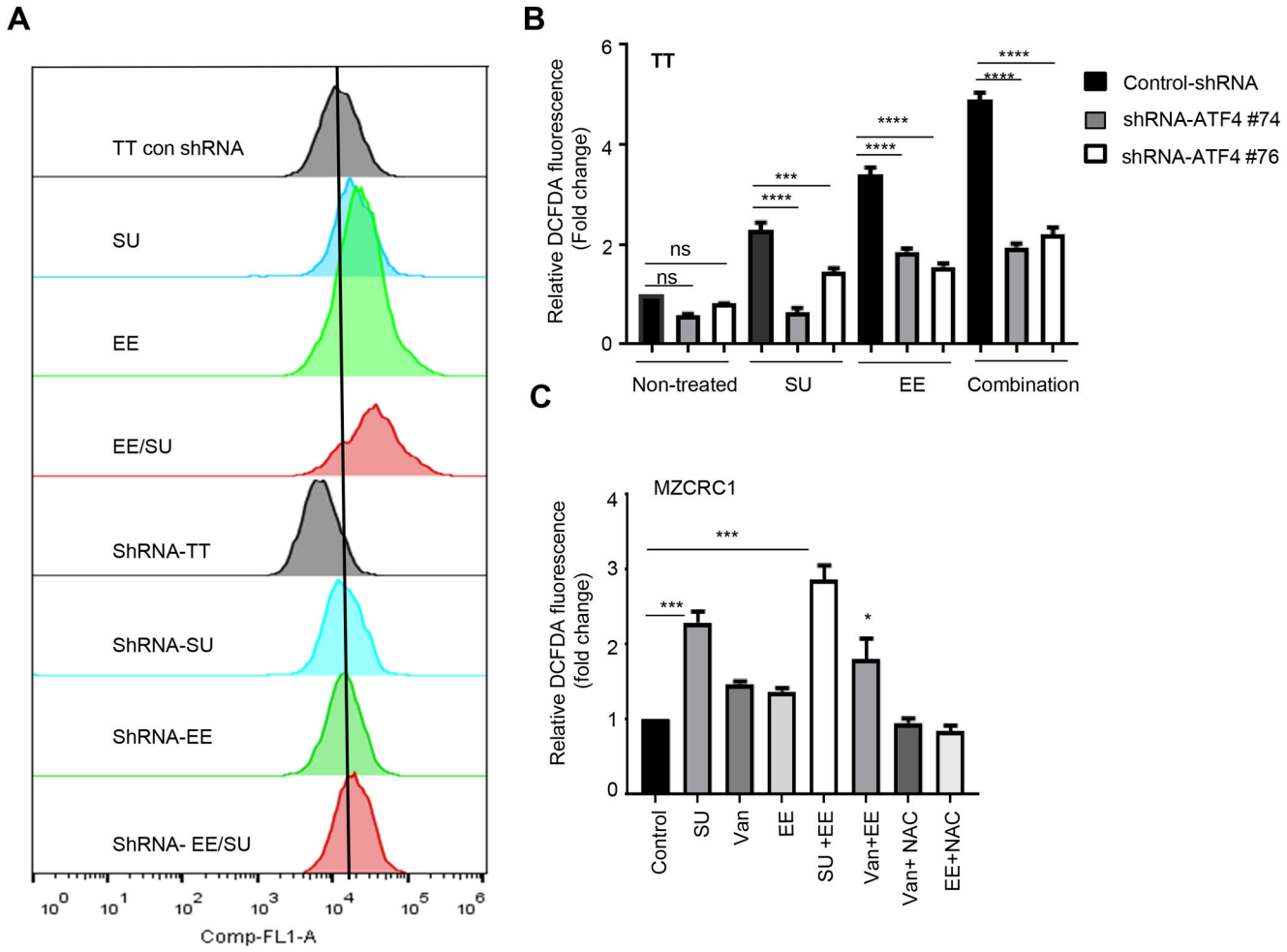

Figure 3.

Eeyarestatin in combination with sunitinib or vandetanib triggers catastrophic oxidative stress. **A**-**B**, ATF4 depletion by shRNA prevents ROS production by sunitinib, eeyarestatin, or their combination. Cells were treated with vehicle, eeyarestatin (4 μM), sunitinib (4 μM), or their combination for 24 h; stained with carboxy-H2DFDA and then subjected to FACS analysis to determine intracellular ROS. One representative experiment is shown in A. Results in B are presented as fold increase in mean fluorescence intensity normalized to untreated and mean of three independent experiment ±SD. **C,** MZCRC1 cells treated with sunitinib (SU), vandetanib (VAN), eeyaresatin (EE), or combinations were stained with DCFDA and then subjected to FACS analysis. Results are presented as fold increase in mean fluorescence intensity normalized to untreated and mean of three independent experiment ±SD. Unpaired two-tailed t-test. *p<0.05, ***p<0.001.

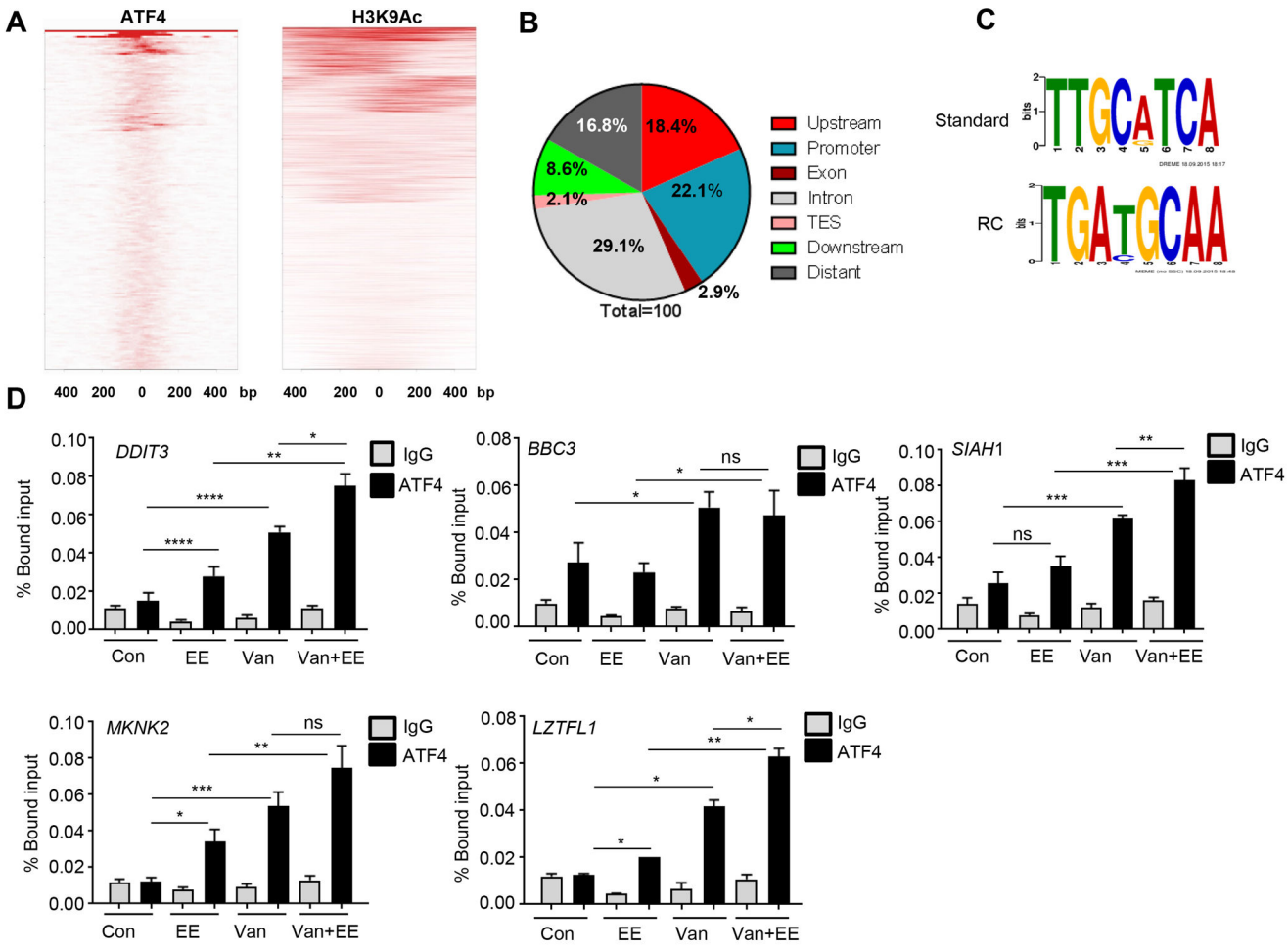

Figure 4.

Genome wide mapping of ATF4 direct target genes identified by ChIP-seq analysis in MZCRC1 cells treated with eeyarestatin (10μM) for 8h. **A,** ChIP-seq density heat map representation of promoter occupancy (400 bp) flanking transcription start site) for ATF4 and H3K9AC. **B,** Distribution of ATF4 ChIP-seq peaks across the genome. The peaks were classified as within introns, within coding sequence (exon), within promoter region, within transcription end site (TES), upstream or downstream of the transcription start site, or distant in intergenic regions. **C,** ATF4 binding motif identified by MEME-ChIP analyses. RC, Reverse Complement. **D,** Occupancy of ATF4 in the promoter regions of targeted genes. MZCRC1 cells were treated with vandetanib (Van; 5 μM), eeyarestatin (EE; 5 μM), or the two drugs in combination for 16 h and then subjected to ChIP assay (details in Methods).

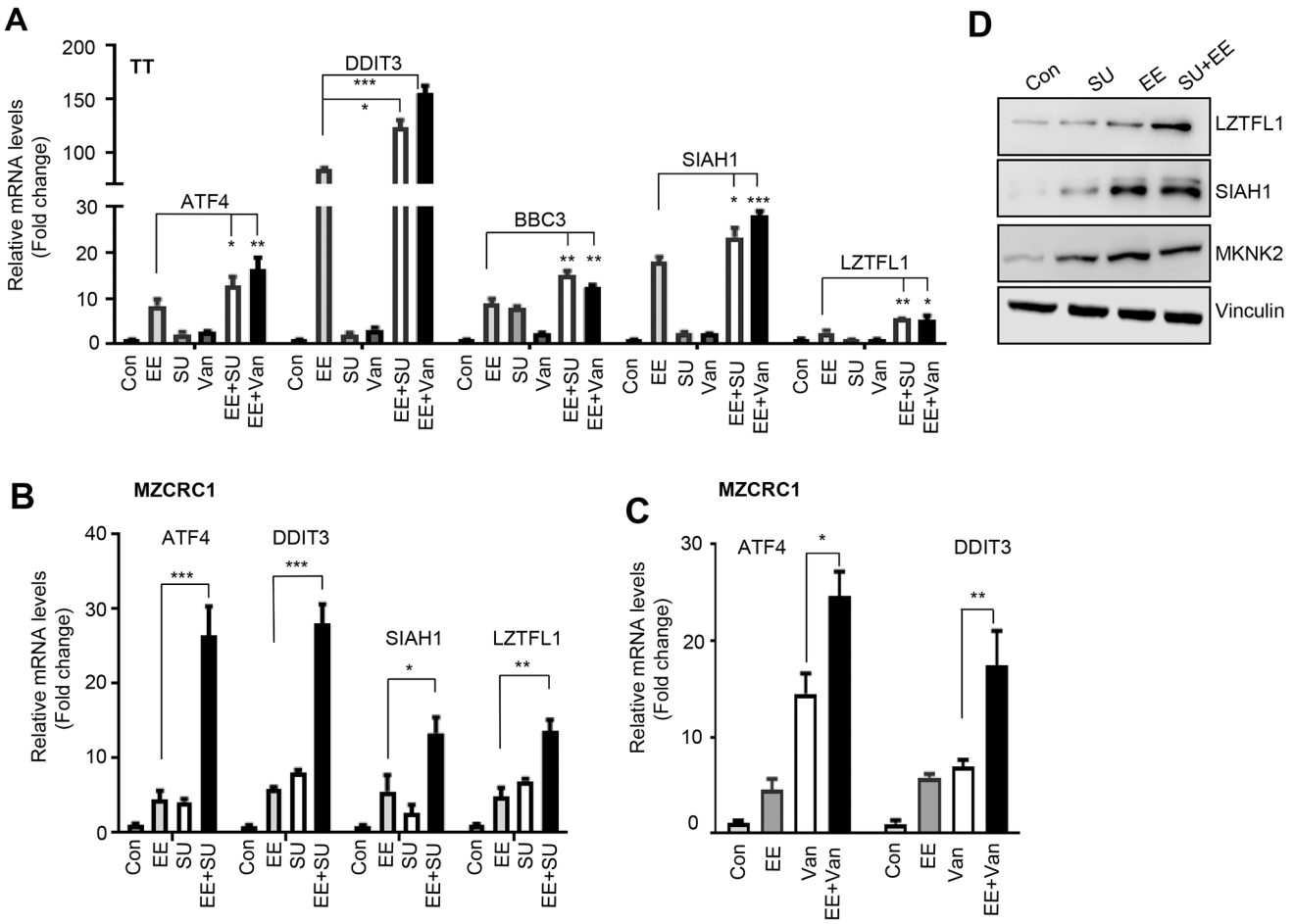

Figure 5.

ATF4 induces the target genes involved in the UPR, apoptosis, transcription, and oxidative stress. **A,** TT cells were treated with vandetanib (Van; 5 μM), eeyarestatin (EE; 5 μM), sunitinib (5μM) or the two drugs in combinations for 16 and gene expression was measured by qRT-PCR using indicated probes and HPRT as an internal control. Data are presented as the mean of three independent experiments ± SD. **B, C** MZCRC1 cells were treated with eeyarestatin (EE; 5 μM), sunitinib (5μM) or vandetanib (Van; 5 μM), or the two drugs in combination for 16 and gene expression was measured by qRT-PCR using indicated probes and HPRT as an internal control. Data are presented as the mean of three independent experiments ± SD. Unpaired two-tailed t-test, *p<0.05, **p< 0.01, ***p<0.001, ****p<0.0001. **D,** MZCRC1 cells treated as in B were analyzed by Western blotting using the indicated antibodies. Vinculin served as a loading control.

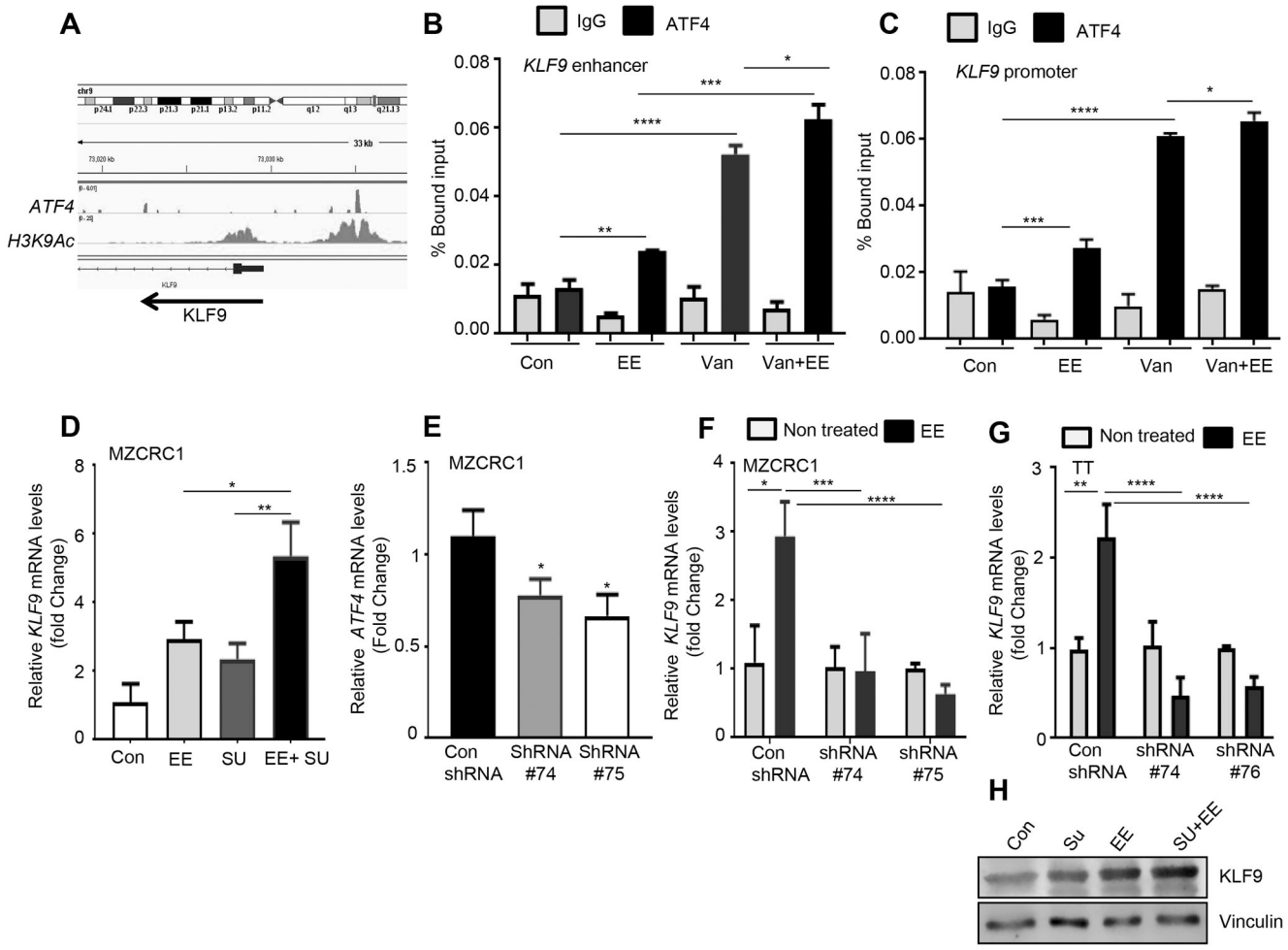

Figure 6.

ATF4 transcriptionally activates KLF9 in response to combination therapy. **A,** Genome browser representation of ChIP-seq peaks for ATF4 and H3K9AC at the KLF9 loci in MZCRC1 cells treated with eeyarestatin. Arrow indicates the direction of transcription. **B, C**, MZCRC1 cells were treated with eeyaresattin 10 μM for 8 h. The chromatin was prepared as described in Material and Methods, precipitated using control (IgG) or ATF4-specific or H3K9AC-specific antibodies and analyzed by qPCR with the indicated primers (see Supplemental Experimental Procedures). **D,** MZCRC1 cells were treated with eeyarestatin (5 μM), sunitinib (5 μM), or the two drugs in combination for 16 h and then subjected to qRT-PCR analysis with KLF9 primer. **E,** Quantitative real-time RT-PCR showing mRNA levels of ATF4 in con shRNA and ATF4 shRNA MZCRC1 cells. **F**, TT control, and TT-shRNA-ATF4 cells were treated with eeyarestatin (5 μM) for 16 h and then subjected to qRT-PCR analysis with KLF9 probe. **G,** MZCRC1 control, and MZCRC1-shRNA-ATF4 cells were treated with eeyarestatin (5 μM) for 16 h and then subjected to qRT-PCR analysis with KLF9 probe. **H,** TT cells treated as in D were analyzed by immunoblotting with the KLF9-specific antibody. Vinculin served as a loading control. Con, control untreated cells; EE, eeyarestatin; Van, vandetanib.